Article

Gas-Phase Preparation of Silyl Cyanide (SiH₃CN) via a Radical Substitution Mechanism

Zhenghai Yang, Chao He, Shane J. Goettl, Dababrata Paul, Ralf I. Kaiser,* Mateus X. Silva, and Breno R. L. Galvão*

Read Online

ACCESS | Metrics & More | Article Recommendations | Supporting Information

ABSTRACT: The silyl cyanide (SiH₃CN) molecule, the simplest representative of a fully saturated silacyanide, was prepared in the gas phase under single-collision conditions via a radical substitution mechanism. The chemical dynamics were direct and revealed a pronounced backward scattering as a consequence of a transition state with a pentacoordinated silicon atom and almost colinear geometry of the attacking cyano radical and leaving hydrogen. Compared to the isovalent cyano (CN)−methane (CH₄) system, the CN−SiH₄ system dramatically reduces the energy of the transition state to silyl cyanide by nearly 100 kJ mol⁻¹, which reveals a profound effect on the chemical bonding and reaction mechanism. In extreme high-temperature environments including circumstellar envelopes of IRC +10216, this versatile radical substitution mechanism may synthesize organosilicon molecules via reactions of silane with doublet radicals. Overall, this study provides rare insights into the exotic reaction mechanisms of main-group XIV elements in extreme environments and affords deeper insights into fundamental molecular mass growth processes involving silicon in our universe.
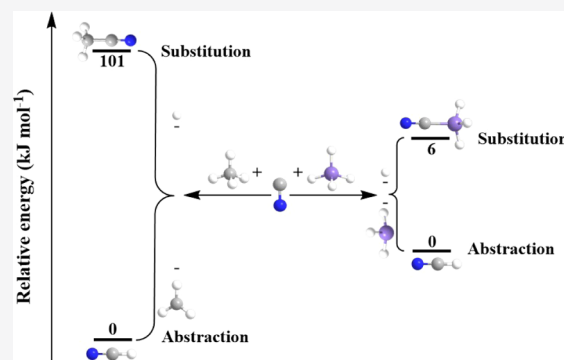
1. INTRODUCTION

Since the discovery of the electrophilic substitution in 1877 by Friedel and Crafts,[1] in which an electrophile (E⁺) displaces a functional group in an organic compound, substitution reaction mechanisms such as nucleophilic (S_N), electrophilic (S_E), and radical (S_R) substitutions[2] play a fundamental role in preparative organic chemistry and in chemical synthesis on the industrial scale.[3−9] From the mechanistic viewpoint, the molecularity of the reaction in the rate-determining step classifies these mechanisms as two-step unimolecular (S_N1, S_E1, S_R1) or one-step bimolecular reactions (S_N2, S_E2, S_R2). These pathways involve reaction complexes containing sp³-hybridized, tetracoordinated carbon atoms or transition states with (distorted) pentacoordinated, trigonal bipyramidal geometries, respectively, as prototype mechanisms for effectively enlarging the molecular complexity of aromatic and aliphatic organic molecules.[5,6,10,11]

In detail, the nucleophile in S_N reaction attacks the carbocation (S_N1) or the carbon atom, which is partially positive (S_N2) emitting a negatively charged leaving group;[6,11] bond making and bond breaking occur in a two-step process (S_N1), where the heterolytic R−X bond dissociation determines the rate constant, or via a one-step process (S_N2) representing one of the most important types of ion−molecule reactions such as in the chloride (Cl⁻)−methyl iodide (CH₃I) system.[11] A wealth of micromechanisms of aliphatic

nucleophilic substitution pathways such as rebound, stripping, and roundabout channels[12] involving Walden inversions at the carbon atom and unexpected spinning of the entire R−X molecule prior to substitution has been studied theoretically[13] and experimentally in the gas phase.[14] In electrophilic substitution reactions involving aliphatic reactants (S_E), the electrophile eventually replaces a functional group. The reactant either heterolytically dissociates into a positively charged group and a carbanion prior to a rapid recombination of the carbanion with the electrophile (S_E1; two-step process) or reacts through a rate-determining, single transition state with the electrophile, together with the simultaneous old bond rupture and the new bond formation (S_E2; one-step process).[15] Although both the nucleophilic (S_N) and electrophilic (S_E) substitution mechanisms have aided in unraveling the physical organic mechanistic framework driving molecular mass growth processes through carbon−carbon bond coupling, the unraveling of dynamics of radical (S_R) substitution reactions in gas phase, also referred to as homolytic radical
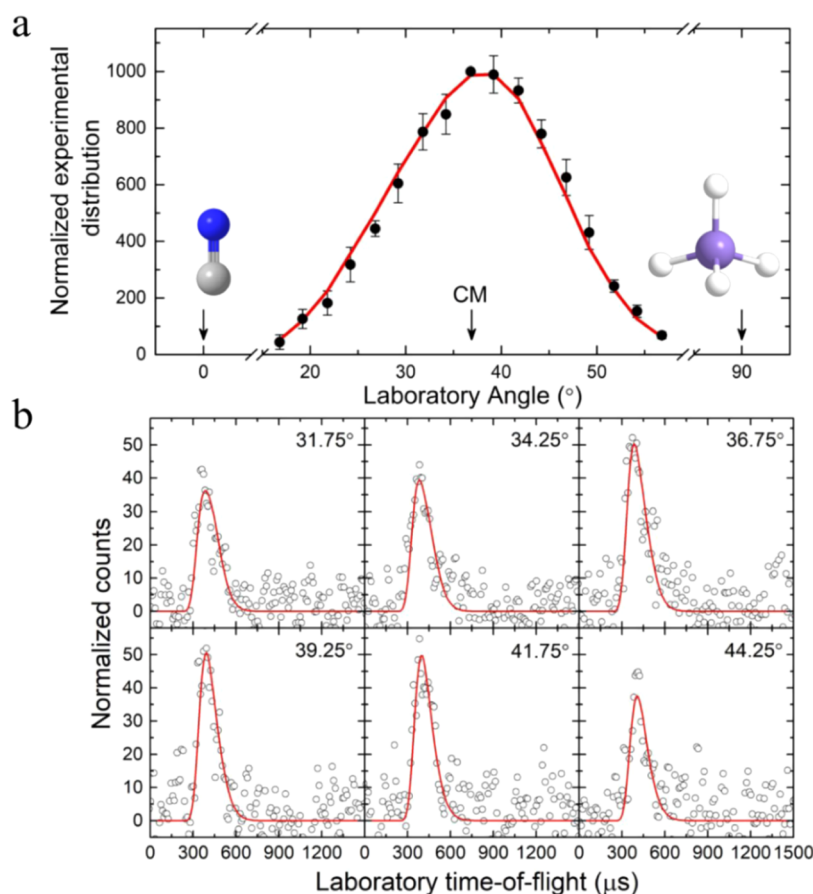
Figure 1. Laboratory angular distribution (a) and time-of-flight spectra (b) (data collected at $m/z = 57$ ($^{28}SiH_3CN^+$)) in the reaction of the cyano radical with silane. The circles represent the experimental results, and the red lines depict the best fits.

substitution reactions, of reactants carrying tetracoordinated carbon or isovalent silicon atoms has been sparse predominantly due to the experimental difficulties in preparing the radical reactants in sufficient concentrations to allow the detection of the nascent reaction products.[16]

In pioneering studies, detailed reactive collision mechanisms were revealed through the simplest hydrogen-atom exchange reaction of atomic hydrogen (H) with molecular hydrogen (H_2);[17,18] Dixon et al.[19] along with Zare et al.,[20] Truhlar et al.,[21] and Zhao et al.[13] unraveled the underlying mechanisms of the reaction of atomic hydrogen (H) with methane (CH_4) or D4-methane (CD_4). A direct hydrogen abstraction pathway forming molecular hydrogen along with the methyl radical (CH_3) was exposed to a barrier of 63 kJ mol^{-1}, which was energetically preferred to the radical substitution channel leading to methane (CH_4) and H with a 159 kJ mol^{-1} barrier.[19] Recently, Rosso et al. explored the gas-phase reaction of germyl (GeH_3)[22] and alkyl radicals[23] with nitrogentrifluoride (NF_3) at pressures from 525 to 700 Torr, demonstrating that the radical substitution mechanism to difluoroaminogermane (GeH_3NF_2) plus atomic fluorine (F) is competitive with the classical abstraction pathway forming fluorogermane (GeH_3F) and the nitrogendifluoride (NF_2) radical.

In main-group 14 elements from carbon (C) to lead (Pb), the valence ns and np orbitals' size increases with some irregularities from d-block contractions (Ge) or relativistic effects (Pb).[24] These orbitals are of central importance in chemical bonding especially in the formation of multiple

bonds.[25,26] For example, heavier elements like silicon show reduced overlap of the valence orbitals and the orthogonality of p orbitals for the increased size of the valence orbitals.[27] As important intermediates in synthetic chemistry, numerous pentacoordinate silicon compounds including pentacoordinate cyanosiliconates,[28] silicon hydride,[29,30] and silicon halides[31] have been studied. Pentacoordinate silicon structures can be formed via addition of an anion, substitution of a trifunctional organosilane, or through a neutral donor inter- or intramolecular coordination.[32] Among these, compounds with fluorine ligands are relatively stable and SiF_5^- is considered a geometrically, electronically, and thermodynamically stable species.[33,34] Besides, pentacoordinated heavy main-group 14 elements including Ge, Sn, and Pb were also investigated.[35−39] However, despite these intriguing discoveries, the fundamental understanding of the reaction dynamics of radical substitution reactions involving reactants carrying tetracoordinated carbon or isovalent silicon atoms and through a pentacoordinated, trigonal bipyramidal transition state under single-collision conditions in the gas phase is still in its infancy. Our crossed molecular beam experiment provides a unique glimpse of the reaction dynamics through the determination of the nascent product translational energy and angular distribution information without wall effects.

Here, exploiting a combined computational and crossed molecular beam investigation, we report the gas-phase formation of silyl cyanide (SiH_3CN) plus atomic hydrogen through a radical substitution pathway (S_R) with a tetracoordinated silicon involving $CN-SiH_4$ bimolecular
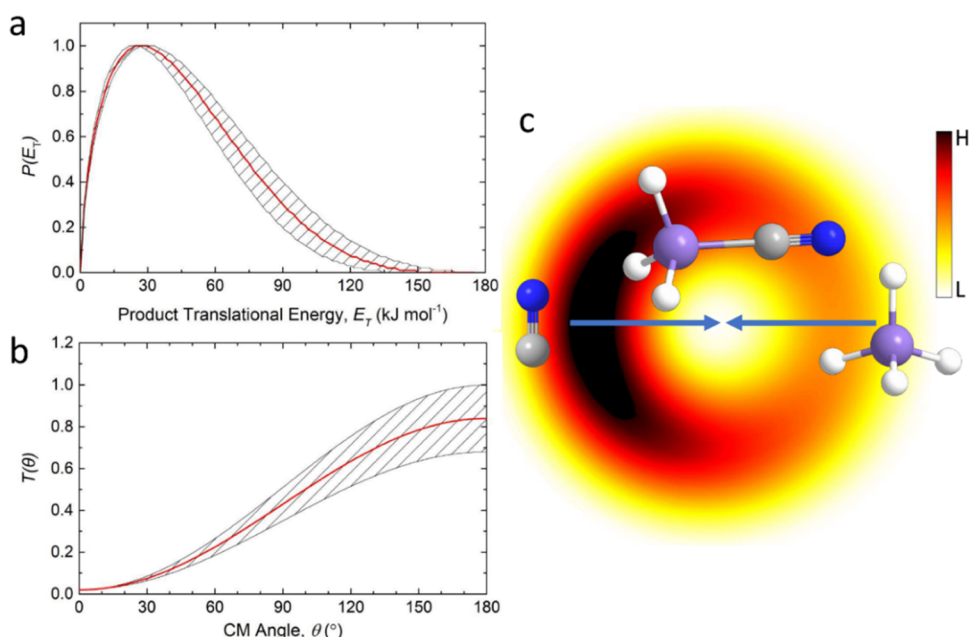
Figure 2. $P(E_T)$ (a), $T(\theta)$ (b) flux distributions along with the corresponding flux contour map (c) for the cyano−silane reaction. The red lines represent the best fit; the shaded areas depict the error limits.

collisions. This elementary reaction forms silyl cyanide (SiH_3CN) through a pentacoordinated silicon atom along with a trigonal bipyramidal transition state containing simultaneous silicon−hydrogen bond rupture and silicon−carbon bond formation. Thus, the cyano−silane system is classified as a prototype reaction with an unusual reactivity of isovalent silicon versus carbon.

$$CN^{\bullet} + SiH_4 \rightarrow SiH_3CN + H^{\bullet} \tag{1}$$
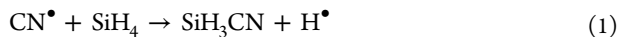
2. RESULTS

2.1. Laboratory Frame. The single-collision signal of the cyano radical (CN, $X^2\Sigma^+$)−silane (SiH_4, X^1A_1) reaction was monitored from m/z 60 ($^{30}SiH_4CN$) to 56 ($^{28}SiH_2CN$, $^{29}SiHCN$, $^{30}SiCN$, $^{28}SiH^{13}CN$, $^{28}SiHC^{15}N$) [^{28}Si (92.2%), ^{29}Si (4.7%), ^{30}Si (3.1), ^{12}C (98.9%), ^{13}C (1.1%), ^{14}N (99.6%), ^{15}N (0.4%)]. No signal from m/z 60 to 58; the time-of-flight (TOF) spectra collected at 57 ($^{28}SiH_3CN$, $^{29}SiH_2CN$, $^{30}SiHCN$, $^{28}SiH_2^{13}CN$, $^{28}SiH_2C^{15}N$) and 56 depict identical patterns after scaling. These findings suggest that no adducts could be detected in the $CN−SiH_4$ system; further, the cyano versus hydrogen-atom exchange pathway forming SiH_3CN (57 amu) along with atomic hydrogen (1 amu) is open under our experimental conditions. The signal observed at $m/z = 56$ is associated with dissociative ionization of the parent product SiH_3CN (57 amu). Note that carbon atoms as well as dicarbon and tricarbon molecules are present in the primary beam and could in principle act as reactants too (5. Experimental Section and Computational Method). However, the reaction products of atomic carbon and dicarbon molecules with silane will lead to the products, which are lower in mass than those formed in the $CN−SiH_4$ reaction and hence do not interfere.[40] Tricarbon molecules were found to be unreactive with silane considering a 21.2 kJ mol^{-1} collision energy. Therefore, the existence of C, C_2, and C_3 in the primary beam will not interfere with the signal detected at 57, and only products formed in the $CN−SiH_4$ reaction contribute to the scattering signal collected. The

scattering signal and TOFs were accumulated at $m/z = 57$ in 2.5° intervals; the ion count ratio of $m/z = 57$ versus $m/z = 56$ was 1.31 ± 0.17:1. TOFs are then normalized to the TOF collected at the CM angle of 37.0 ± 0.5° yielding the laboratory angular distribution (LAD) as shown in Figure 1, which is spread over 40° within the scattering plane and depicts a higher intensity in the backward hemisphere ("backward scattering"). Overall, the laboratory data alone reveal an unusual radical substitution pathway (reaction (1)) leading to SiH_3CN isomer(s). Recall that the QMS operates in the TOF mode; this means that the detection system effectively monitors the product flight time with a well-defined m/z ratio from the collision center to the electron impact ionizer.

2.2. Center-of-Mass Frame. Our laboratory data prove that SiH_3CN is prepared; now it is our goal to expose the corresponding dynamics together with the nature of the formed SiH_3CN isomer(s). To accomplish these objectives, the scattering data were transformed into the CM reference frame (5. Experimental Section and Computational Method) providing eventually the CM translational energy $P(E_T)$ and angular $T(\theta)$ flux distributions, as depicted in Figure 2; the corresponding best fits of the laboratory data are shown in Figure 1, which are derived utilizing a single reaction channel leading to heavy product of 57 amu (SiH_3CN) and the light product of 1 amu (H); a reaction threshold of 12 ± 5 kJ mol^{-1} was incorporated into the fitting routine. This transformation provided key information on the reaction mechanism. First, the $P(E_T)$ holds a maximum translational energy release E_{max} of 150 ± 16 kJ mol^{-1}. For those products born without internal excitation, E_{max} denotes the sum of the collision energy plus the reaction exoergicity. This results in a reaction exoergicity of −132 ± 16 kJ mol^{-1}. Second, the $P(E_T)$ peaks at 27 ± 3 kJ mol^{-1}, which is away from zero translational energy, suggesting a tight transition state resulting in the product isomer(s). Third, the average translational energy was revealed to be 46 ± 5 kJ mol^{-1} indicating a release of only 31 ± 6% of the maximum energy into the product translational degrees of
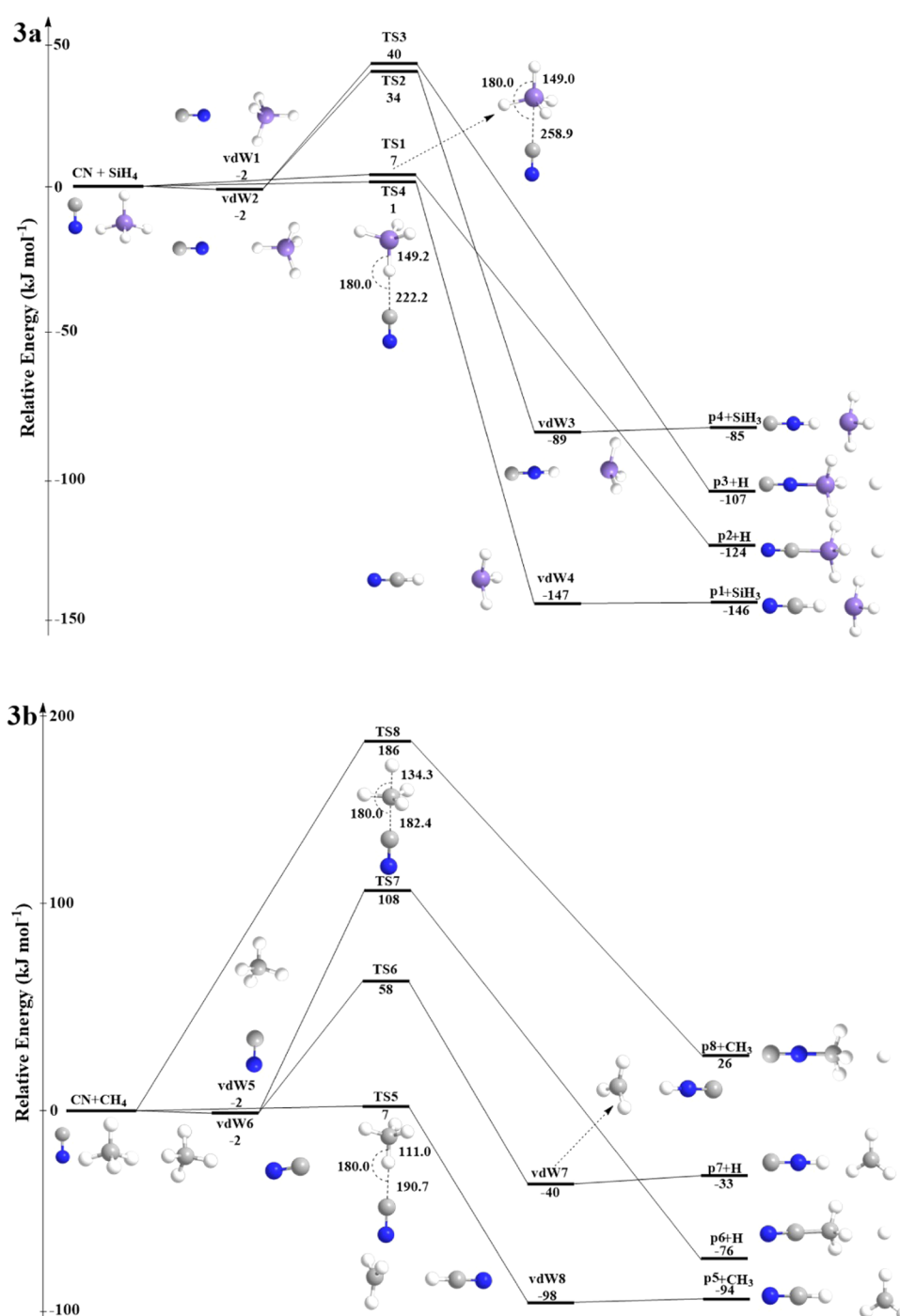
Figure 3. Potential energy surface (PES) for the reactions of the cyano radical with silane (3a) and methane (3b). Bond angles and bond lengths are given in degrees and picometers, respectively. **TS4** is calculated by Burke et al. (see ref 45). Colors of the atoms: carbon (gray), silicon (purple), nitrogen (blue), and hydrogen (white).

freedom. Further, the $T(\theta)$ flux distribution monotonically increases with the scattering angle from 0 to 180° with a pronounced intensity maximum at 180°. This finding indicates "backward scattering" dynamics and rebound dynamics involving a direct reaction through a single transition state connecting the reactants to the products. These findings are also visualized in the flux contour map (Figure 2c), which depicts the reactive scattering product flux intensity as a function of the CM scattering angle and product velocity; this distribution can be seen as an image of the reaction and contains all information on the scattering process.[41]

3. DISCUSSION

The formation of SiH_3CN isomer(s) via direct reaction dynamics (backward scattering) has been identified; we are now incorporating the results above with electronic structure calculations, which can help reveal the nature of the formed isomer(s) and the corresponding formation mechanisms in the $CN-SiH_4$ system. The computations were carried out with relative energies of the transition states, and local minima were calculated with explicitly correlated calculations that usually provide accuracies within 8 kJ mol^{-1} (Figure 3a).[42,43] Relative

D

energies (reactants, intermediates, transition states, products) are shown in Figure 3a. The calculations identified four reaction channels. These include two classical abstraction channels leading to hydrogen cyanide (**p1**, HCN) and hydrogen isocyanide (**p4**, HNC) plus the silyl radical (SiH$_3$); the difference in the reaction energies of 61 kJ mol^{-1} agrees well with the differences in enthalpies of formation of hydrogen cyanide versus hydrogen isocyanide of 62 kJ mol^{-1}.[44] In addition, two radical substitution (S$_R$) channels forming silyl cyanide (**p2**, SiH$_3$CN) and silyl isocyanide (**p3**, SiH$_3$NC) plus atomic hydrogen (H) were located.

Recall that a rection energy of -132 ± 16 kJ mol^{-1} has been experimentally determined; here, the calculation results indicate that the formation of the thermodynamically most stable silyl cyanide (**p2**, SiH$_3$CN) isomer is preferred in the cyano radical and silane reaction. How is this molecule formed? The computations reveal a one-step radical substitution (S$_R$) pathway, in which a single transition state **TS1** connects the cyano radical and silane reactants with the silyl cyanide (**p2**, SiH$_3$CN) and atomic hydrogen (H) products. This transition-state barrier is much lower than the collision energy (7 kJ mol^{-1} versus 18.2 ± 0.5 kJ mol^{-1}) and can be overcome easily in the experiment. The computed transition-state structure reveals a pentacoordinated silicon atom holding a trigonal bipyramidal geometry, where the cyano radical is set at one of the apices. This results in a nearly collinear (180°) geometry of the axial Si−H bond with the cyano radical and a simultaneous bond-forming−bond-breaking process (Table 1).

Table 1. Comparison of Geometric Parameters of TS1 and TS7 with the Reactants (X = C, Si). A Pentacoordinated Silicon Atom Holding a Trigonal Bipyramidal Geometry is Revealed in TS1

species	C−N (pm)	C−X (pm)	X−H (pm)	H−X−C (degree)
CN	117.3			
SiH$_4$			147.6	
CH$_4$			108.6	
TS1	117.1	258.9	149.0 (axial)	180.0
TS7	116.3	182.4	134.3 (axial)	180.0

The nearly collinear geometry of the transition state supports our experimental findings of a "backward scattering" (Figures 1 and 2) through direct scattering dynamics in which the cyano radicals form a carbon−silicon bond with the silicon atom at low (nearly zero) impact parameters resulting in back-scattered heavy silyl cyanide (**p2**, SiH$_3$CN) reaction product. Considering the low barrier of only 7 kJ mol^{-1} for **TS1**, at elevated temperatures, this radical substitution pathway can compete with the classical abstraction channel passing a reaction barrier of only 1 kJ mol^{-1} to form hydrogen cyanide (**p1**, HCN) plus the silyl radical.[45] Rate constant calculations computed using TST (transition-state theory) within RRHO (rigid rotor-harmonic oscillator) approximation with Eckart's tunneling correction reveal rapid reaction rates for the bimolecular radical substitution pathway of 1.6×10^{-11}, 5.4×10^{-11}, and 1.2×10^{-10} cm^3 s^{-1} at 1000, 1500, and 2000 K, respectively, compared to typical rates in the order of 9.2×10^{-13} cm^3 s^{-1} for the classical abstraction pathway to hydrogen cyanide (**p1**, HCN) at 1000 K.[45] The Skodje−Truhlar[46] tunneling corrections were also computed, with both results agreeing within 1% (Figure 4).
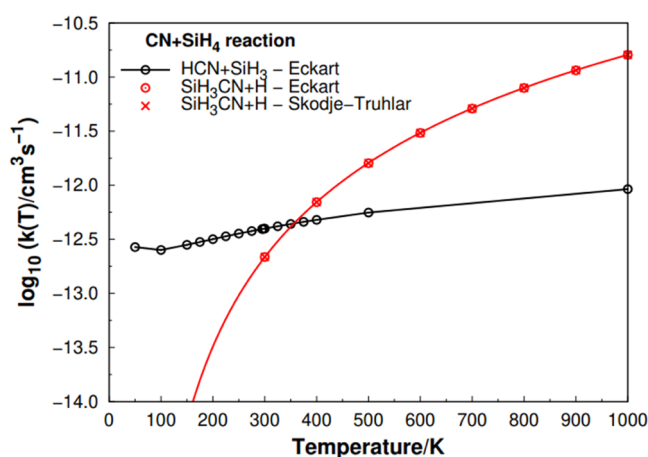

Figure 4. Temperature dependence of rate constants of CN + SiH$_4$ → SiH$_3$CN + H (calculated in this work) and CN + SiH$_4$ → HCN + SiH$_3$ (extracted from Burke et al.) reactions. The labels "Eckart" and "Skodje−Truhlar" refer to the tunneling correction method.

Do alternative reaction pathways exist? The calculations predict two reaction pathways leading to silyl isocyanide (**p3**, SiH$_3$NC) plus atomic hydrogen (H) and hydrogen isocyanide (**p4**, HNC) plus the silyl radical (SiH$_3$). These pathways are initiated through the existence of the van der Waals complexes, which are weakly bound (-2 kJ mol^{-1}), in which the nitrogen atom points to the silicon (**vdW1**) and a hydrogen atom (**vdW2**). These complexes pass through transition states **TS3** and **TS2** eventually forming silyl isocyanide (**p3**, SiH$_3$NC) plus atomic hydrogen (H) and hydrogen isocyanide (**p4**, HNC) plus the silyl radical (SiH$_3$). Considering that both transition states are higher than 18.2 kJ mol^{-1}, the pathways to silyl isocyanide (**p3**, SiH$_3$NC) and hydrogen isocyanide (**p4**, HNC) are both closed. Overall, our investigations prove that silyl cyanide (**p2**, SiH$_3$CN) is formed through direct (backward scattering) reaction dynamics and a radical substitution pathway involving a pentacoordinated silicon atom in the reaction, which is overall exoergic ($\Delta_R G = -124$ kJ mol^{-1}) and rapid (1.2×10^{-10} cm^3 s^{-1} at 2000 K) at elevated temperatures. This outcome is quite distinct from the classically "expected" reaction pathway leading solely to hydrogen cyanide (**p1**, HCN) plus the silyl radical via a direct abstraction process.

It is attractive to contrast the elucidated reaction mechanisms of the CN−SiH$_4$ system with those of the isovalent reaction of the cyano radical with methane (CH$_4$). The computational investigation also unraveled four channels in this carbon-based chemistry with the calculated relative energy shown in Figure 3b. These include two classical hydrogen abstraction pathways leading to hydrogen cyanide (**p5**, HCN) and hydrogen isocyanide (**p7**, HNC) along with the methyl radical (CH$_3$). Further, two radical substitution channels forming methyl cyanide (**p6**, CH$_3$CN,) and methyl isocyanide (**p8**, CH$_3$NC) together with atomic hydrogen were identified. However, the thermodynamically most stable product methyl cyanide (**p6**, CH$_3$CN) via the radical substitution pathway is only accessible through a transition state (**TS7**) with a high barrier of 108 kJ mol^{-1}. This radical substitution pathway is, hence, closed. However, the classical hydrogen abstraction channel leading to hydrogen cyanide (**p5**, HCN) only has to pass a transition state (**TS5**) with a 7 kJ mol^{-1} barrier, which is much preferred. Remarkably, the

energy difference in these transition states of 101 kJ mol^{-1} in the CN−CH$_4$ system is reduced by 95 kJ mol^{-1} to only 6 kJ mol^{-1} in the CN−SiH$_4$ system. The frontier orbitals of the transition states of the radical substitution on silane (**TS1**) are compared to those on methane (**TS7**) in Figure 5. Silicon has
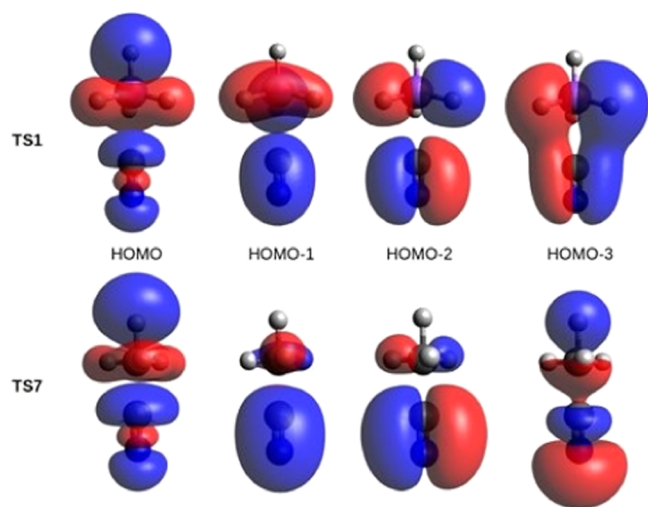

Figure 5. Frontier molecular orbitals for the transition states of the radical substitution mechanism on silane (**TS1**) and methane (**TS7**).

a larger covalent radius, lower electronegativity, and vacant 3d orbitals compared to carbon[47] and tends to expand its valence shell to pentacoordination forming stable compounds with increased electropositive character considering the vacant d orbitals, the effect of σ^* (Si−L) orbitals with high p character, and the three-center four-electron bonding.[48−51] This results in a higher barrier (108 kJ mol^{-1}) in carbon-based chemistry compared to the silane−cyano system (7 kJ mol^{-1}).

Therefore, the replacement of a tetravalent carbon atom by an isoelectronic silicon atom in the methane molecule has a profound impact on the reaction dynamics and opens up a competitive radical substitution pathway to the astronomically observed silyl cyanide (**p2**, SiH$_3$CN) molecule.[52,53]

4. CONCLUSIONS

The elementary cyano−silane gas-phase reaction forming silyl cyanide (SiH$_3$CN) and atomic hydrogen (H) was explored by exploiting molecular beam experiments and electronic structure calculations. The direct chemical dynamics were revealed and exposed a radical substitution mechanism via a single transition state containing a pentacoordinated silicon atom with a nearly colinear geometry of the attacking cyano radical, the forming carbon−silicon bond, along with the cleaving silicon−hydrogen moiety. The reaction dynamics are distinct when comparing to the dynamics of the isovalent cyano−methane system, which is dictated solely by hydrogen abstraction, indicating that insights into the reaction mechanisms of carbon systems cannot readily predict the chemical dynamics of the isovalent silicon system. Overall, the cyano−silane reaction represents a one-step radical substitution mechanism benchmark in the gas phase involving the coupling of a silicon−carbon bond leading to new insights into the dynamics of radical substitution mechanisms at tetravalent silicon atoms and how they compare to the isovalent carbon systems.

This silicon−carbon bond formation that proves to be facile in our crossed molecular beam experiments holds important implications for extraterrestrial chemistry. Although silyl cyanide (SiH$_3$CN) has been identified in the circumstellar envelope of IRC + 10216, previously its gas-phase synthesis has remained rather uncertain. Speculative ion−molecule reactions involving CH$_3$CNH$^+$ and SiH$_3$CNH$^+$ were eventually ruled out based on recent Atacama Large Millimeter/submillimeter Array (ALMA) observations.[54] Hypothetical catalytic reactions on the surface of silicon−carbon grains were discounted too.[52,53] However, considering temperatures of a few 1000 K in those regions close to the central star, the transition state of 7 kJ mol^{-1} of the exoergic gas-phase substitution reaction of the cyano radical with silane leading to silyl cyanide (SiH$_3$CN) can be easily overcome and could provide a versatile synthetic route to incorporate silyl moieties into organosilicon molecules. Utilizing macroscopic environments such as circumstellar envelopes of carbon-rich AGB stars as a natural laboratory, the study of radical substitution mechanisms on the microscopic, molecular level involving silane (SiH$_4$) leads us to predict the formation of silyl acetylene (SiH$_3$CCH), methylsilane (CH$_3$SiH$_3$), and 1-silylpropyne (CH$_3$CCSiH$_3$) via reactions of silane with ethynyl (C$_2$H), methyl (CH$_3$), and 1-propynyl (CCCH$_3$) radicals. Overall, the silicon−carbon bonds formed here via radical substitution pathways at chemical and physical conditions representing circumstellar envelopes close to the star such as IRC + 10216 deepen our understanding of the exotic reaction mechanisms and chemistry in these extreme environments and assist deeper insights into fundamental molecular mass growth processes involving silicon in the molecular universe we live in.[53,54]

5. EXPERIMENTAL SECTION AND COMPUTATIONAL METHODS

5.1. Experimental Section. The molecular-level gas-phase reaction of the cyano radical (CN, X$^2\Sigma^+$) with silane (SiH$_4$, X^{1}A$_1$) was investigated with a crossed molecular beam machine.[55] The primary supersonic cyano beam was generated in situ by laser ablation of a graphite rod with a 266 nm Nd:YAG laser (30 Hz, 10−12 mJ pulse^{-1}). The ablated species were seeded in nitrous oxide (N$_2$O, Matheson, 99.999%), which also acted as a reactant gas and was released by a pulse valve (60 Hz, 4 atm). The pulsed primary CN radical beam was velocity-selected by a chopper wheel located prior to the interaction region, yielding a ν_p (peak velocity) of 1350 ± 24 m s^{-1} and S (speed ratio) of 3.7 ± 0.2 (Table S1). In the interaction region, the primary pulse crossed the secondary pure silane (SiH$_4$, Linde, 99.999%) beam with ν_p of 827 ± 20 m s^{-1} and S of 10.1 ± 0.2 perpendicularly, resulting in a collision energy of 18.2 ± 0.5 kJ mol^{-1} along with a center-of-mass (CM) angle of 37.0 ± 0.5°. An electron impact ionizer was used to ionize the reactive scattering products at an ultrahigh vacuum of around 8 × 10^{-12} Torr.[56] The scattering signal was mass-filtered and angularly resolved utilizing a triply differentially pumped QMS (quadrupole mass spectrometer) in the time-of-flight (TOF) mode and eventually recorded using a Daly-type ion counter.[57] The laboratory angular distribution (LAD) at a selected mass to charge (m/z) was obtained by integrating the TOF spectra at different angles and scaling to the intensity at the CM angle. The laboratory data of the TOF spectra and the LAD were transformed into the CM frame exploiting a forward-convolution routine to reveal the reaction dynamics information including the CM translational energy $P(E_T)$ and the angular $T(\theta)$ flux distributions.[58,59] The fitting procedure starts with the initial prediction of CM functions to fit the laboratory data iteratively until reaching the best fits. The $I(\theta, u)$, i.e., reactive differential cross section, which can be separated into CM angle θ and velocity u as $I(\theta, u) \sim P(u) \times T(\theta)$, is presented as a flux contour map containing the scattering process information.[41]

5.2. Computational Methods. All electronic structure calculations presented in this work were carried out with the MOLPRO[60] and ORCA[61,62] packages. Geometry optimizations of reactants, products, intermediates, and transition states concerning both SiH_4 + CN and CH_4 + CN reactions were performed with density functional theory (DFT)[63] and the B2PLYP-D3 double hybrid density functional with Grimme's dispersion correction and Becke–Johnson damping[64,65] and with the cc-pV(T + d)Z basis set.[66] No symmetry restriction was enforced in any geometry optimization. A vibrational analysis was performed on all obtained stationary points at the same B2PLYP-D3/cc-pV(T + d)Z level. Stationary points assigned as potential energy minima were confirmed to possess only real vibrational frequencies, while a single imaginary frequency was obtained for the transition states (TSs). To assign the connecting structures for each TS, intrinsic reaction coordinate (IRC) calculations were performed. Localized molecular orbitals according to Pipek−Mezey (population−localization) are also at the DFT level of theory. For each optimized structure, single-point energy calculations were performed at the explicitly correlated RCCSD(T)-F12/cc-pVTZ-F12[43,67] level using the MOLPRO software to achieve higher accuracy on the energy values. The reaction energies and barrier heights are hereafter termed as CCSD(T)-F12/cc-pVTZ-F12//B2PLYP-D3/cc-pV(T + d)Z + ZPE(B2PLYP-D3/cc-pV(T + d)Z). Specifically for the optimized van der Waals intermediates, we also performed an anharmonic vibrational analysis according to second-order vibrational perturbation theory as implemented in ORCA. This was carried out at the ωB97X-D3BJ/ cc-pV(T + d)Z level,[68,69] and the anharmonic correction was added to the ZPE previously obtained for these intermediates at the B2PLYP-D3/cc-pV(T + d)Z level. Finally, rate constants were computed using transition-state theory (TST) within the rigid rotor-harmonic oscillator (RRHO) using energies and molecular parameters from the electronic structure calculations. The Eckart[70−72] and Skodje−Truhlar[46] tunneling corrections were computed. The MESS software package was employed for the calculations.[73]

ASSOCIATED CONTENT

⑤ Supporting Information

The Supporting Information is available free of charge at https://pubs.acs.org/doi/10.1021/jacs.2c01349.

Experimental parameters (Table S1), comparison of our calculated results with experimental results (Table S2), calculated coordinates and vibrational frequencies involved in the CN−SiH_4 (Table S3), and CN−CH_4 (Table S4) reactions (PDF)

AUTHOR INFORMATION

Corresponding Authors

Ralf I. Kaiser − *Department of Chemistry, University of Hawai'i at Manoa, Honolulu, Hawaii 96822, United States;* ⓘ orcid.org/0000-0002-7233-7206; Email: ralfk@hawaii.edu

Breno R. L. Galvão − *Centro Federal de Educação Tecnológica de Minas Gerais, CEFET-MG, 30421-169 Belo Horizonte, Minas Gerais, Brazil;* ⓘ orcid.org/0000-0002-4184-2437; Email: brenogalvao@gmail.com

Authors

Zhenghai Yang − *Department of Chemistry, University of Hawai'i at Manoa, Honolulu, Hawaii 96822, United States*

Chao He − *Department of Chemistry, University of Hawai'i at Manoa, Honolulu, Hawaii 96822, United States*

Shane J. Goettl − *Department of Chemistry, University of Hawai'i at Manoa, Honolulu, Hawaii 96822, United States;* ⓘ orcid.org/0000-0003-1796-5725

Dababrata Paul − *Department of Chemistry, University of Hawai'i at Manoa, Honolulu, Hawaii 96822, United States*

Mateus X. Silva − *Centro Federal de Educação Tecnológica de Minas Gerais, CEFET-MG, 30421-169 Belo Horizonte, Minas Gerais, Brazil;* ⓘ orcid.org/0000-0001-9629-3829

Complete contact information is available at: https://pubs.acs.org/10.1021/jacs.2c01349

Notes

The authors declare no competing financial interest.
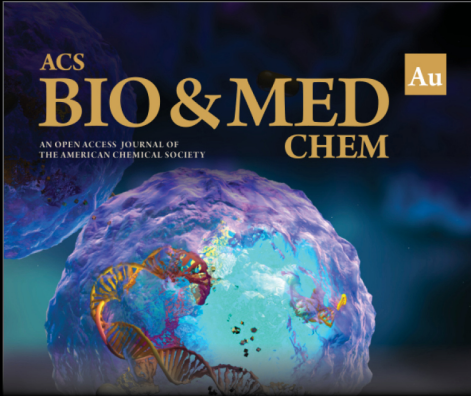
REFERENCES

(1) Friedel, C.; Crafts, J.-M. Sur une nouvelle méthode générale de synthèse d'hydrocarbures, d'acétones, etc. *Compt. Rend.* **1877**, *84*, 1392−1395.

(2) S_R is also sometimes called homolytic S_H.

(3) Cowdrey, W. A.; Hughes, E. D.; Ingold, C. K.; Masterman, S.; Scott, A. D. 257. Reaction Kinetics and the Walden Inversion. Part VI. Relation of Steric Orientation to Mechanism in Substitutions Involving Halogen Atoms and Simple or Substituted Hydroxyl Groups. *J. Chem. Soc.* **1937**, 1252−1271.

(4) Ingold, C. K. *Structure and Mechanism in Organic Chemistry*; Cornell University Press: Ithaca, NY, 1953.

(5) Mortier, J. *Arene Chemistry: Reaction Mechanisms and Methods for Aromatic Compounds*; John Wiley & Sons: Hoboken, NJ, 2016.

(6) Arnaut, L.; Burrows, H. *Chemical Kinetics: From Molecular Structure to Chemical Reactivity*; Elsevier, 2006.

(7) Fossey, J.; Lefort, D.; Sorba, J. *Free Radicals in Organic Chemistry*; John Wiley and Sons, 1995.

(8) Lowry, T. H.; Richardson, K. S. *Mechanism and Theory in Organic Chemistry*; Harper & Row, 1987.

(9) Liljenberg, M.; Brinck, T.; Herschend, B.; Rein, T.; Rockwell, G.; Svensson, M. Validation of a Computational Model for Predicting the Site for Electrophilic Substitution in Aromatic Systems. *J. Org. Chem.* **2010**, *75*, 4696−4705.

(10) Hartshorn, S. R. *Aliphatic Nucleophilic Substitution*; Cambridge University Press: London, 1973.

(11) Mikosch, J.; Trippel, S.; Eichhorn, C.; Otto, R.; Lourderaj, U.; Zhang, J. X.; Hase, W. L.; Weidemüller, M.; Wester, R. Imaging Nucleophilic Substitution Dynamics. *Science* **2008**, *319*, 183−186.

(12) Xie, J.; Hase, W. L. Rethinking the S_N2 Reaction. *Science* **2016**, *352*, 32−33.

(13) Zhao, Z.; Zhang, Z.; Liu, S.; Zhang, D. H. Dynamical Barrier and Isotope Effects in the Simplest Substitution Reaction via Walden Inversion Mechanism. *Nat. Commun.* **2017**, *8*, No. 14506.

(14) Stei, M.; Carrascosa, E.; Kainz, M. A.; Kelkar, A. H.; Meyer, J.; Szabó, I.; Czakó, G.; Wester, R. Influence of the Leaving Group on the Dynamics of a Gas-Phase S_N2 Reaction. *Nat. Chem.* **2016**, *8*, 151−156.

(15) Fukuto, J. M.; Jensen, F. R. Mechanisms of S_E2 Reactions: Emphasis on Organotin Compounds. *Acc. Chem. Res.* **1983**, *16*, 177−184.

(16) Lucas, M.; Thomas, A. M.; Yang, T.; Kaiser, R. I.; Mebel, A. M.; Hait, D.; Head-Gordon, M. Bimolecular Reaction Dynamics in the Phenyl−Silane System: Exploring the Prototype of a Radical Substitution Mechanism. *J. Phys. Chem. Lett.* **2018**, *9*, 5135−5142.

(17) Aoiz, F. J.; Bañares, L.; Herrero, V. J. The H+H$_2$ Reactive System. Progress in the Study of the Dynamics of the Simplest Reaction. *Int. Rev. Phys. Chem.* **2005**, *24*, 119−190.

(18) Harich, S. A.; Dai, D.; Wang, C. C.; Yang, X.; Chao, S. D.; Skodje, R. T. Forward scattering due to slow-down of the intermediate in the H+HD→D+H$_2$ reaction. *Nature* **2002**, *419*, 281−284.

(19) Dobbs, K. D.; Dixon, D. A. Ab initio prediction of the activation energies for the abstraction and exchange reactions of H with CH$_4$ and SiH$_4$. *J. Phys. Chem. A* **1994**, *98*, 5290−5297.

(20) Camden, J. P.; Bechtel, H. A.; Zare, R. N. Dynamics of the Simplest Reaction of a Carbon Atom in a Tetrahedral Environment. *Angew. Chem., Int. Ed.* **2003**, *42*, 5227−5230.

(21) Albu, T. V.; Espinosa-García, J.; Truhlar, D. G. Computational Chemistry of Polyatomic Reaction Kinetics and Dynamics: The Quest for an Accurate CH$_5$ Potential Energy Surface. *Chem. Rev.* **2007**, *107*, 5101−5132.

(22) Antoniotti, P.; Benzi, P.; Marabello, D.; Rosso, D. Experimental and Theoretical Study on the Gas-Phase Reactions of Germyl Radicals with NF$_3$: Homolytic Substitution at the Nitrogen Atom vs Fluorine Abstraction. *ACS Omega* **2020**, *5*, 4907−4914.

(23) Antoniotti, P.; Benzi, P.; Borocci, S.; Demaria, C.; Giordani, M.; Grandinetti, F.; Operti, L.; Rabezzana, R. Bimolecular Homolytic Substitutions at Nitrogen: An Experimental and Theoretical Study on the Gas-Phase Reactions of Alkyl Radicals with NF$_3$. *Chem. - Eur. J.* **2015**, *21*, 15826−15834.

(24) Pyykko, P. Relativistic Effects in Structural Chemistry. *Chem. Rev.* **1988**, *88*, 563−594.

(25) Nagase, S.; Kobayashi, K.; Takagi, N. Triple Bonds between Heavier Group 14 Elements. A Theoretical Approach. *J. Organomet. Chem.* **2000**, *611*, 264−271.

(26) Fischer, R. C.; Power, P. P. π-Bonding and the Lone Pair Effect in Multiple Bonds Involving Heavier Main Group Elements: Developments in the New Millennium. *Chem. Rev.* **2010**, *110*, 3877−3923.

(27) Kutzelnigg, W. Chemical Bonding in Higher Main Group Elements. *Angew. Chem., Int. Ed.* **1984**, *23*, 272−295.

(28) Dixon, D. A.; Hertler, W. R.; Chase, D. B.; Farnham, W. B.; Davidson, F. Pentacoordinate Cyanosiliconates. *Inorg. Chem.* **1988**, *27*, 4012−4018.

(29) Sini, G.; Ohanessian, G.; Hiberty, P. C.; Shaik, S. S. Why is SiH$_5^-$ a Stable Intermediate while CH$_5^-$ is a Transition State? A Quantitative Curve Crossing Valence Bond Study. *J. Am. Chem. Soc.* **1990**, *112*, 1407−1413.

(30) Hajdasz, D. J.; Ho, Y.; Squires, R. R. Gas-phase Chemistry of Pentacoordinate Silicon Hydride Ions. *J. Am. Chem. Soc.* **1994**, *116*, 10751−10760.

(31) Gutsev, G.; Boldyrev, A. DVM-Xα Calculations on the Ionization Potentials of MX$_{k+1}^-$ Complex Anions and the Electron Affinities of MX$_{k+1}$ "Superhalogens". *Chem. Phys.* **1981**, *56*, 277−283.

(32) Chuit, C.; Corriu, R. J. P.; Reye, C.; Young, J. C. Reactivity of Penta- and Hexacoordinate Silicon Compounds and Their Role as Reaction Intermediates. *Chem. Rev.* **1993**, *93*, 1371−1448.

(33) Marchaj, M.; Freza, S.; Skurski, P. Why Are SiX$_5^-$ and GeX$_5^-$ (X= F, Cl) Stable but Not CF$_5^-$ and CCl$_5^-$? *J. Phys. Chem. A* **2012**, *116*, 1966−1973.

(34) Ault, B. S. Infrared Matrix Isolation Studies of the M$^+$SiF$_5^-$ Ion Pair and Its Chlorine-Fluorine Analogs. *Inorg. Chem.* **1979**, *18*, 3339−3343.

(35) Takeuchi, Y.; Tanaka, K.; Tanaka, K.; Ohnishi-Kameyama, M.; Kálmán, A.; Párkányi, L. Synthesis and Structure of a Novel Pentacoordinate Organogermanium Compound. *Chem. Commun.* **1998**, 2289−2290.

(36) Bharadwaj, P. K.; Arbuckle, B. W.; Musker, W. K. Structure of a Novel Neutral Lead (II) Complex with Dipropyldithiocarbamate. *Inorg. Chim. Acta* **1988**, *142*, 243−246.

(37) Reich, H. J.; Phillips, N. H. Lithium Pentaalkyl/aryl Stannate Complexes as Intermediates in the Lithium-tin Exchange Reaction. *Pure Appl. Chem.* **1987**, *59*, 1021−1026.

(38) Baukov, Y. I.; Tandura, S. N. Hypervalent Compounds of Organic Germanium, Tin and Lead Derivatives. In *The Chemistry of Organic Germanium, Tin and Lead Compounds*; Rappoport, Z., Eds.; John Wiley & Sons, Inc., 2002; Vol. 2, pp 963−1239.

(39) Carroll, M. T.; Gordon, M. S.; Windus, T. L. Hypercoordination in Group IV MH$_5$ and MH$_5^-$ systems. *Inorg. Chem.* **1992**, *31*, 825−829.

(40) Rettig, A.; Head-Gordon, M.; Doddipatla, S.; Yang, Z.; Kaiser, R. I. Crossed Beam Experiments and Computational Studies of Pathways to the Preparation of Singlet Ethynylsilylene (HCCSiH; X^{1}A′): The Silacarbene Counterpart of Triplet Propargylene (HCCCH; X^{3}B). *J. Phys. Chem. Lett.* **2021**, *12*, 10768−10776.

(41) Levine, R. D. *Molecular Reaction Dynamics*; Cambridge University Press, 2005.

(42) Zhang, J.; Valeev, E. F. Prediction of reaction barriers and thermochemical properties with explicitly correlated coupled-cluster methods: A basis set assessment. *J. Chem. Theory Comput.* **2012**, *8*, 3175−3186.

(43) Adler, T. B.; Knizia, G.; Werner, H.-J. A Simple and Efficient CCSD (T)-F12 Approximation. *J. Chem. Phys.* **2007**, *127*, No. 221106.

(44) He, C.; Yang, Z.; Doddipatla, S.; Zhao, L.; Goettl, S.; Kaiser, R. I.; Silva, M. X.; Galvão, B. R. Non-Adiabatic Reaction Dynamics in the Gas-Phase Formation of Phosphinidenesilylene, the Isovalent Counterpart of Hydrogen Isocyanide, under Single-Collision Conditions. *J. Phys. Chem. Lett.* **2021**, *12*, 2489−2495.

(45) Burke, A. D.; Bowman, M. C.; Turney, J. M.; Schaefer, H. F. Energetics and Kinetics of Various Cyano Radical Hydrogen Abstractions. *Phys. Chem. Chem. Phys.* **2021**, *23*, 3389−3400.

(46) Skodje, R. T.; Truhlar, D. G. Parabolic Tunneling Calculations. *J. Phys. Chem. B* **1981**, *85*, 624−628.

(47) Tandura, S. N.; Voronkov, M. G.; Alekseev, N. V. *Molecular and Electronic Structure of Penta-and Hexacoordinate Silicon Compounds*; Springer, 1986.

(48) Dilman, A. D.; Ioffe, S. L. Carbon−Carbon Bond Forming Reactions Mediated by Silicon Lewis Acids. *Chem. Rev.* **2003**, *103*, 733−772.

(49) Schomburg, D.; Krebs, R. Structural Chemistry of Pentacoordinated Silicon. Molecular Structures of the Pentafluorosilicate Anion and the Diphenyltrifluorosilicate Anion. *Inorg. Chem.* **1984**, *23*, 1378−1381.

(50) Pimentel, G. C. The Bonding of Trihalide and Bifluoride Ions by the Molecular Orbital Method. *J. Chem. Phys.* **1951**, *19*, 446−448.

(51) Hach, R. J.; Rundle, R. E. The Structure of Tetramethylammonium Pentaiodide. *J. Am. Chem. Soc.* **1951**, *73*, 4321−4324.

(52) Agúndez, M.; Cernicharo, J.; Guélin, M. New Molecules in IRC +10216: Confirmation of C$_5$S and Tentative Identification of MgCCH, NCCP, and SiH$_3$CN. *Astron. Astrophys.* **2014**, *570*, A45.

(53) Cernicharo, J.; Agúndez, M.; Prieto, L. V.; Guélin, M.; Pardo, J. R.; Kahane, C.; Marka, C.; Kramer, C.; Navarro, S.; Quintana-Lacaci, G.; et al. Discovery of Methyl Silane and Confirmation of Silyl Cyanide in IRC+10216. *Astron. Astrophys.* **2017**, *606*, L5.

(54) Agúndez, M.; Cernicharo, J.; Quintana-Lacaci, G.; Prieto, L. V.; Castro-Carrizo, A.; Marcelino, N.; Guélin, M. The Peculiar Distribution of CH$_3$CN in IRC+10216 Seen by ALMA. *Astrophys. J.* **2015**, *814*, 143.

(55) Gu, X.; Guo, Y.; Zhang, F.; Mebel, A. M.; Kaiser, R. I. Reaction Dynamics of Carbon-Bearing Radicals in Circumstellar Envelopes of Carbon Stars. *Faraday Discuss.* **2006**, *133*, 245−275.

(56) Brink, G. O. Electron Bombardment Molecular Beam Detector. *Rev. Sci. Instrum.* **1966**, *37*, 857−860.

(57) Daly, N. R. Scintillation Type Mass Spectrometer Ion Detector. *Rev. Sci. Instrum.* **1960**, *31*, 264−267.

(58) Vernon, M. F. *Molecular Beam Scattering*; University of California: Berkeley, CA, 1983.

(59) Weiss, P. S. *The Reaction Dynamics of Electronically Excited Alkali Atoms with Simple Molecules*; University of California: Berkeley, CA, 1986.

(60) Werner, H. J.; Knowles, P. J.; Knizia, G.; Manby, F. R.; Schütz, M.; Celani, P.; Györffy, W.; Kats, D.; Korona, T.; Lindh, R.. *MOLPRO*, Version 2015.1, a Package of Ab Initio Programs; University of Cardiff Chemistry Consultants (UC3): Cardiff, Wales, UK, 2015.

(61) Neese, F. The ORCA Program System. *Wiley Interdiscip. Rev.: Comput. Mol. Sci.* **2012**, *2*, 73−78.

(62) Neese, F. Software Update: the ORCA Program System, Version 4.0. *Wiley Interdiscip. Rev.: Comput. Mol. Sci.* **2018**, *8*, No. e1327.

(63) Kohn, W.; Sham, L. J. Self-Consistent Equations Including Exchange and Correlation Effects. *Phys. Rev.* **1965**, *140*, A1133−A1138.

(64) Grimme, S. Semiempirical Hybrid Density Functional with Perturbative Second-Order Correlation. *J. Chem. Phys.* **2006**, *124*, No. 034108.

(65) Grimme, S.; Antony, J.; Ehrlich, S.; Krieg, H. A Consistent and Accurate Ab Initio Parametrization of Density Functional Dispersion Correction (DFT-D) for the 94 Elements H-Pu. *J. Chem. Phys.* **2010**, *132*, No. 154104.

(66) Dunning, T. H.; Peterson, K. A.; Wilson, A. K. Gaussian Basis Sets for Use in Correlated Molecular Calculations. X. The Atoms Aluminum Through Argon Revisited. *J. Chem. Phys.* **2001**, *114*, 9244−9253.

(67) Knizia, G.; Adler, T. B.; Werner, H.-J. Simplified CCSD (T)-F12 Methods: Theory and Benchmarks. *J. Chem. Phys.* **2009**, *130*, No. 054104.

(68) Lin, Y.-S.; Li, G.-D.; Mao, S.-P.; Chai, J.-D. Long-Range Corrected Hybrid Density Functionals with Improved Dispersion Corrections. *J. Chem. Theory Comput.* **2013**, *9*, 263−272.

(69) Najibi, A.; Goerigk, L. The Nonlocal Kernel in van der Waals Density Functionals as an Additive Correction: An Extensive Analysis with Special Emphasis on the B97M-V and ωB97M-V Approaches. *J. Chem. Theory Comput.* **2018**, *14*, 5725−5738.

(70) Pople, J. A.; Schlegel, H. B.; Krishnan, R.; Defrees, D. J.; Binkley, J. S.; Frisch, M. J.; Whiteside, R. A.; Hout, R. F.; Hehre, W. J. Molecular Orbital Studies of Vibrational Frequencies. *Int. J. Quantum Chem.* **2009**, *20*, 269−278.

(71) Ribeiro, J. M.; Mebel, A. M. Reaction Mechanism and Rate Constants of the CH+CH$_4$ Reaction: A Theoretical Study. *Mol. Phys.* **2015**, *113*, 1865−1872.

(72) Truhlar, D. G.; Garrett, B. C.; Klippenstein, S. J. Current Status of Transition-State Theory. *J. Phys. Chem. C* **1996**, *100*, 12771−12800.

(73) Georgievskii, Y.; Klippenstein, S. J. *MESS Program Package*, 2015.